JBC RESEARCH ARTICLE

In vivo pulse-chase in *Caenorhabditis elegans* reveals intestinal histone turnover changes upon starvation

Received for publication, February 17, 2025, and in revised form, April 26, 2025 Published, Papers in Press, May 27, 2025,
https://doi.org/10.1016/j.jbc.2025.110299

Christopher Borchers[1,2], **Kara Osburn**[1], **Hyun Cheol Roh**[1], **and Scott T. Aoki**[1,*]

From the [1]*Department of Biochemistry and Molecular Biology, School of Medicine; Indiana University Indianapolis, Indianapolis, Indiana, USA; and* [2]*Indiana BioMedical Gateway (IBMG) Program, School of Medicine, Indiana University Indianapolis, Indianapolis, Indiana, USA*

Reviewed by members of the JBC Editorial Board. Edited by Joseph Jez

The ability to study protein dynamics and function in the authentic context of a multicellular organism is paramount to better understand biological phenomena in animal health and disease. Pulse-chase of self-labeling fusion protein tags provides the opportunity to label proteins of interest and track those proteins over time. There are currently several challenges associated with performing *in vivo* protein pulse-chase in animals, such as cost, reproducibility, and accurate detection methods. The *Caenorhabditis elegans* model organism has attributes that alleviate many of these challenges. This work tests the feasibility of applying the Halo modified enzyme (HaloTag) for *in vivo* protein pulse-chase in *C. elegans*. HaloTag intestinal histone reporters were created in the worm and used to demonstrate that reporter protein could be efficiently pulse-labeled by soaking animals in ligand. Labeled protein stability could be monitored over time by fluorescent confocal microscopy. Further investigation revealed reporter protein stability was dependent on the animal's nutritional state. Chromatin immunoprecipitation and sequencing of the reporters showed incorporation in chromatin with little change hours into starvation, implying a lack of chromatin regulation at the time point tested. Collectively, this work presents a straightforward method to label and track proteins of interest in *C. elegans* that can address a multitude of biological questions surrounding protein stability and dynamics in this animal model.

Life relies on a concerted orchestra of biological processes, with proteins as the primary workhorse. Proteins must perform specific functions and then be degraded when no longer required. Aberrant mutation or expression of proteins can have profound impacts on health and disease (1). Thus, developing methods to dissect protein dynamics are critical to understand the basic molecular mechanisms that govern life.

Protein pulse-chase is a versatile tool that can be used to study protein dynamics in cells and multicellular organisms. Original protein-pulse chase methods involved global, nonspecific labeling of proteins using heavy or radioactive isotopes of amino acids (2–5). Although this strategy can assess global protein stability, the spatial expression and dynamics across tissues is lost. The development of modified enzyme tags enable targeted protein *in vivo* pulse-chase (6–8). HaloTag is a modified *Rhodococcus rhodochrous* haloalkane dehalogenase with a mutation that traps the enzyme substrate as a covalent intermediate (9). Its fluorescent ligand signal is more stable and less sensitive to fixatives compared to conventional fluorescent tags (9, 10). Covalent bond formation allows saturated labeling and enzyme-ligand stability, enabling HaloTag and its ligands to function in pulse-chase methods. In this strategy, the "pulse" occurs during enzyme crosslinking to free ligand. Proteins can be "chased" by tracking the complex over time. HaloTag has reportedly higher fluorescent signal to other modified enzyme tags (10, 11), and there are many commercially available HaloTag ligands, allowing flexibility for different labeling strategies. Thus, HaloTag technology is highly amenable for targeted protein pulse-chase applications.

HaloTag-based *in vivo* pulse-chase methods have been previously used to study protein stability in cell culture (6, 7, 12, 13) and in mice (8, 14). Although informative, cell culture studies lack the true context of authentic tissue in living organisms. Conducting HaloTag pulse-chase in organisms like mice involves both economic and technical challenges. The high cost and large quantities of Halo ligands required present significant financial barriers.

Caenorhabditis elegans is an established model organism with advantageous characteristics for *in vivo* pulse-chase methods. Site-specific gene editing methods are well-established to easily add single-copy reporters or tag endogenous genes. The animal has a fast generational life cycle, well understood responses to different biological environments, and a transparent body for straightforward imaging (15). Some tissues in *C. elegans* are easily recognizable by light microscopy and thus do not need additional markers to identify them. For example, the intestine of *C. elegans* is a large, distinct, highly dynamic tissue that serves as an animal's contact to the outside world. In addition to its primary role in metabolism, the intestine functions in immunity, protein secretion, and metal detoxification (16–20). At hatching, larvae have 20 intestinal cells (21) that undergo cell division and endoreduplication to produce 30 to 34 nuclei with a DNA

* For correspondence: Scott T. Aoki, staoki@iu.edu.

© 2025 THE AUTHORS. Published by Elsevier Inc on behalf of American Society for Biochemistry and Molecular Biology. This is an open access article under the CC BY license (http://creativecommons.org/licenses/by/4.0/).

content of 32C, or 16 times more than a normal diploid nucleus (22, 23). Like all metazoans, this DNA is organized through chromatin organization by histones, nuclear proteins that compact DNA and play a central role in gene expression (24). The core repeating unit of chromatin is the nucleosome, an octamer of histone subtypes by which DNA is wound around (25). The *C. elegans* core histones share significant sequence identity to the human counterparts (26). Furthermore, many histone modifications and chromatin remodeling factors are conserved across metazoans, from worms to humans, implying organisms share significant chromatin biology (26). Metabolic changes have been associated with dynamic changes in chromatin structure (27, 28), illustrating histones and chromatin play a critical role maintaining metabolic homeostasis.

This work explores the feasibility of performing *in vivo* pulse-chase in *C. elegans*. HaloTag intestinal histone protein reporters were designed and could be labeled *in vivo* for imaging-based monitoring. Stability of labeled histone proteins changed with nutritional stress. The histone reporter proteins incorporated into chromatin, implying use in gene regulation. Collectively, this work illustrates the potential of *C. elegans* pulse-chase to study protein dynamics and function in animal biology and pathology.

Results

In vivo *pulse labeling of intestinal histone reporters*

The overarching goal was to develop a strategy to track the tissue specific stability of a target protein to determine its lifespan *in vivo*. Histone proteins were selected due to the extensive research of their assembly and function, and the *C. elegans* intestine selected due to its strikingly large nuclei and high DNA content in adult worms (22) (Fig. 1*A*). Intestinal histone reporters were created using MosSCI gene editing (29) to insert a single copy of a reporter gene (Fig. 1*B*, see Experimental procedures). The reporters consisted of an intestinal *elt-2* promoter (30); *his-58*, *his-9*, or *his-72*; a V5 epitope (31) and HaloTag (9), and an *unc-54* 3′UTR (Fig. 1*B*). The three histone variants were chosen due to their unique functions and conservation across metazoans. *his-58* is a canonical H2B protein and a core nucleosome component (24). *his-9* and *his-72* are histone H3 variants that are commonly associated with gene repression and expression, respectively (24). The transgenes enabled tissue specific expression with identical gene regulatory elements. Thus, all protein expression level differences observed between histones would be due to inherent properties of the protein, not other factors associated with posttranscriptional regulation. Histone reporter worms fixed

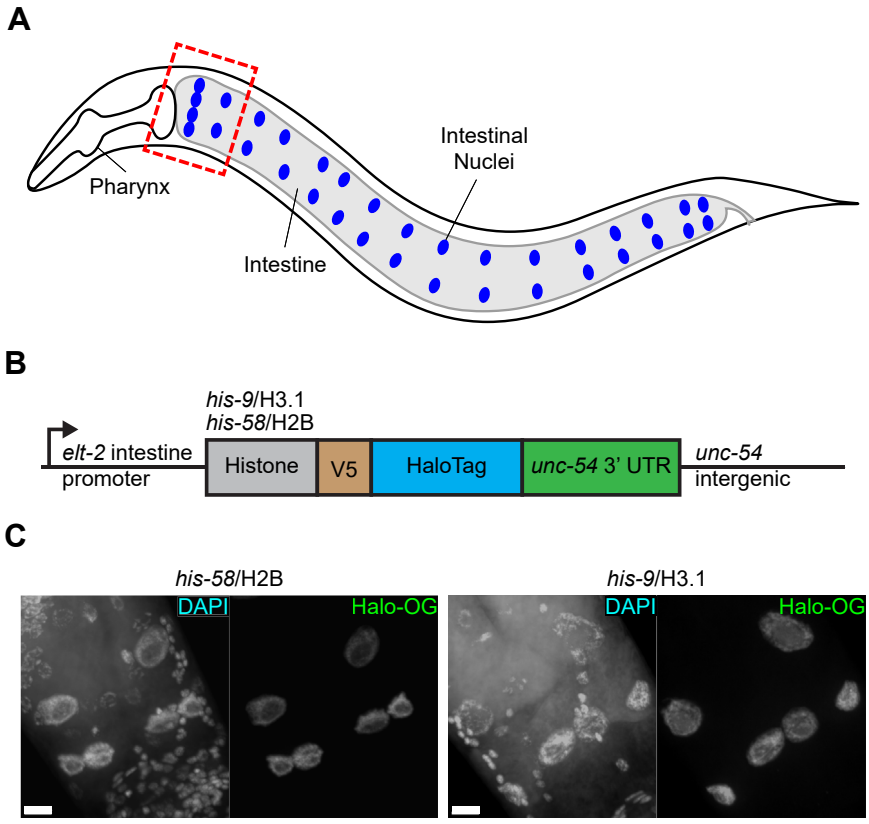

Figure 1. Intestinal histone reporters are robustly expressed. *A*, diagram of adult *Caenorhabditis elegans* intestinal nuclei. Animals have 20 intestinal cells and 30 to 34 nuclei (*blue*, 34 shown). *Dashed box* outlines intestinal region of interest in this study. *B*, linear diagram of the HaloTag intestinal histone reporter. An *elt-2* intestine-specific promoter drives histone variants fused to a V5 epitope and HaloTag in *C. elegans*. All reporters also have an *unc-54* 3′UTR and intergenic region. *C*, confocal images of histone reporter variant strains. Worms were stained with DAPI to visualize nuclei and Halo-Oregon Green (Halo-OG) visualize reporter protein. Images taken of the anterior portion of the intestine at 63× magnification under oil immersion and shown as max intensity projection of confocal stack. The scale bar represents 10 μm. DAPI, 4′,6-diamidino-2-phenylindole.

and stained with Halo-ligand showed specific expression in intestinal nuclei (Fig. 1*C*), as expected of histones. Of note, *his-58*/H2B and *his-9*/H3.1 reporters showed robust fluorescence (Fig. 1*C*), while *his-72*/H3.3 had fainter signal (Fig. S1*A*). This difference in histone protein expression was also observed by immunoblot (Fig. S1, *B* and *C*). *his-9*/H3.1 and *his-72*/H3.3 differ by only nine amino acids (Fig. S1*D*), but the proteins had significantly different protein expression levels. Due to the equivalent protein expression and research goals, the remainder of the study focused on using the *his-58*/H2B and *his-9*/H3.1 reporters to test protein labeling and tracking *in vivo*.

The HaloTag enzyme variant covalently binds to haloalkane ligands (9). As demonstrated in cells (6, 7, 12, 13) and multicellular organisms (8, 14), fluorescent ligands can be pulsed to label tagged proteins. To test this system in *C. elegans*, *his-58*/H2B reporter worms were soaked in different fluorescent HaloTag ligands, washed, fixed, counterstained with a different HaloTag ligand, and imaged by confocal microscopy (Fig. S2*A*). Worms pulse-labeled with the Halo-TMR ligand had significantly higher fluorescence compared to the other ligands tested (Fig. S2, *A* and *B*). Pulse-labeled reporter worms were next evaluated for their efficiency in labeling nuclei throughout the intestine. *his-58*/H2B reporter worms were soaked with Halo-TMR, washed, fixed, counterstained, and the whole worm imaged by confocal microscopy (Fig. S3*A*). Although the intestinal histone reporter was uniformly expressed throughout the intestine (Fig. S3, *A* and *B*), Halo-TMR fluorescence signal was highest in nuclei at the anterior and posterior regions (Fig. S3, *A* and *B*). *C. elegans* have 30 to 34 intestinal nuclei, with variation dependent on variable division of the posterior nuclei (21, 22). Subsequent pulse-chase imaging experiments focused on the anterior intestinal nuclei to avoid this variability. In sum, this pulse-labeling strategy with Halo-TMR ligand enabled tissue-specific protein labeling. The strong fluorescent signal created the opportunity to test whether the labeling method could be used to follow protein stability over time.

To assess the feasibility of *in vivo* pulse-chase with the HaloTag in *C. elegans*, young adult *his-58*/H2B and *his-9*/H3.1 reporter worms were pulse-incubated with Halo-TMR ligand and then allowed to propagate on bacterial plates for several hours before collection, fixing, staining, and imaging (Fig. 2*A*, see Experimental procedures). Worms that were either not pulse-labeled or collected immediately after labeling served as negative and positive controls, respectively. As observed previously, both *his-58*/H2B and *his-9*/H3.1 reporter protein were labeled with Halo-TMR ligand in worms at appreciable levels compared to controls (Fig. 2, *B* and *C*; Fig. S4, *A* and *B*). By 3 h, Halo-TMR signal was significantly lost, reaching basal levels (Fig. 2, *B* and *C*; Fig. S4, *A*, *B* and *D*). Counterstaining of the reporters with a separate fluorescent ligand confirmed that the reporter was expressed in all worm samples (Fig. 2*B*; Fig. S4, *A* and D). These findings demonstrate that the propagation of pulse-labeled animals lead to the loss of the pulse-labeled protein signal in *C. elegans*.

A concern was that the loss of signal observed was solely due to photobleaching or other confounders not connected to biology. As a control, an additional HaloTag nuclear protein in the intestine was pursued. Nuclear lamins are intermediate filament proteins that assemble the nuclear lamina, a structure that connects the nuclear envelope to chromatin (32). Lamins help sequester heterochromatin to the nuclear periphery and function in gene regulation (32). The proteins are stable in the intestine tissue, with an estimated half-life of 5 days in mice (33). *C. elegans* have one lamin gene, *lmn-1* (34). An LMN-1 intestinal reporter was generated by MosSCI single gene editing (29) (Fig. S5*A*). The reporter design was similar to the other intestinal reporters, with an *elt-2* promoter (30), *lmn-1* exons and introns, V5 epitope (31), HaloTag (9), and *unc-54* 3′UTR and intergenic region (Fig. S5*A*). Intestinal *his-58*/H2B and LMN-1 reporters were pulse-labeled by soaking worms in Halo-TMR, followed by washing and immediate collection or collection after 3-h on bacteria-containing plates (Fig. S5*B*). Worms were fixed, counterstained, and imaged by confocal microscopy. Fluorescence quantitation revealed that the mean fluorescence intensity was similar between *his-58*/H2B and LMN-1 reporters immediately after pulse-labeling (Fig. S5, *C* and *D*). However, after a 3-h chase, the fluorescence intensity of the LMN-1 reporter was higher compared to the *his-58*/H2B reporter (Fig. S5, *C* and *D*). This result suggested that the LMN-1 reporter protein was more stable than histone H2B and provided supportive evidence that Halo tag pulse-chase method detected different protein stability with different proteins *in vivo*.

Previous studies demonstrated that starving worms affected chromatin in nonintestinal cell types (35). To probe the pulse-chase method further, reporter worms were starved to examine how nutritional stress influenced labeled protein stability. Young adult *his-58*/H2B and *his-9*/H3.1 reporter worms were starved prior to *in vivo* pulse-chase labeling and chasing in the absence of bacterial food (Fig. 2*A*, see Experimental procedures). As performed previously, nonpulsed worms and worms collected immediately after pulse-labeling served as negative and positive controls, respectively. Starved reporter worms expressed the HaloTag histone reporters at comparable levels as fed worms, measured by immunoblot (Fig. S1, *B* and *C*), and were effectively pulse-labeled, determined by imaging (Fig. 2, *B* and *D*; Fig. S4, *A* and *C*). However, instead of returning to basal levels as seen in fed animals (Fig. 2, *B* and *C*; Fig. S4, *A*, *B*, and *D*), starved animals retained appreciable levels of pulse-labeled histone reporter protein signal (Fig. 2, *B* and *D*; Fig. S4, *A*, *C*, and *D*). Collectively, the results suggested that the stability of reporter histone proteins were influenced by the animal's nutritional status.

Histone reporter proteins incorporate into chromatin

A concern using the histone reporters was their utility in the intestine. Although the reporter histones colocalized with DNA in intestinal nuclei (Fig. 1), it was unclear if the proteins were deposited into chromatin for use in gene regulation. To probe functionality, chromatin immunoprecipitation and

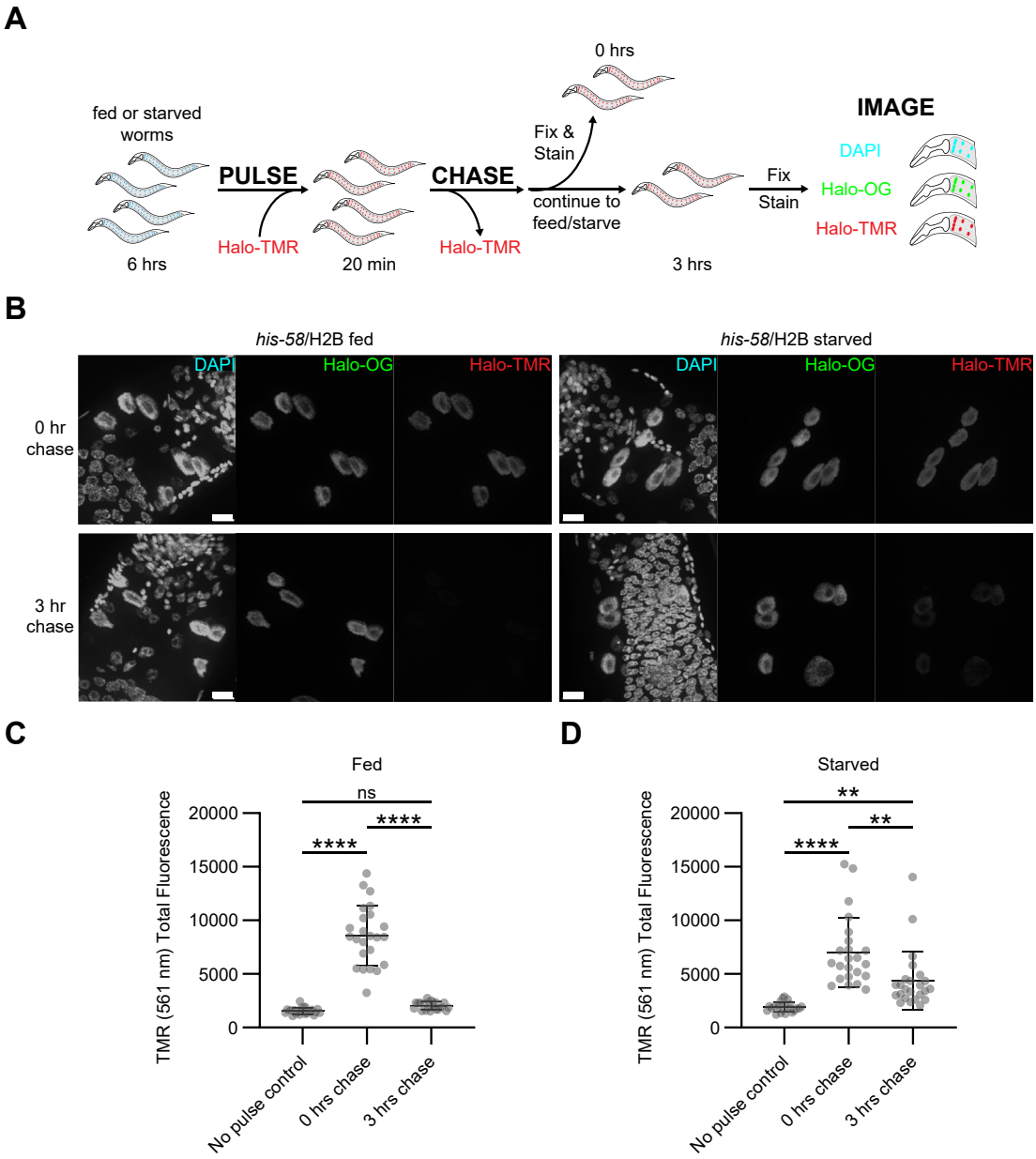

Figure 2. *In vivo* labeling of intestinal histone reporters. *A*, *in vivo* HaloTag pulse-chase method. Intestinal histone reporter animals were pulse-labeled by soaking in the presence of Halo-TMR ligand. Animals were washed and allowed to propagate for 0 or 3 h. At each time point, animals were collected, fixed, stained with DAPI (DNA) and Halo-Oregon Green (Halo-OG), and imaged using confocal microscopy to assess fluorescence intensity over time. *B*, representative images of fed and starved *his-58*/H2B reporter anterior intestinal nuclei after a 0- or 3-h chase. Images shown as max intensity projection of confocal stack taken at 63× magnification under oil immersion. The scale bar represents 10 μM. *C* and *D*, fluorescence intensity measurements of fed (*C*) and starved (*D*) *his-58*/H2B reporter anterior nuclei. Each data point represents an independent biological replicate. Fluorescence was significantly higher after a 3-h chase when compared to a no pulse control. Significance was determined by performing a one-way ANOVA with Tukey's multiple comparisons test; $^{**}p < 0.01$; $^{****}p < 0.0001$; ns, not significant; DAPI, 4′,6-diamidino-2-phenylindole.

sequencing (ChIP-seq) was performed on fed or starved adult worms (36, 37) (Fig. 3*A*). After a 6-h period of feeding or starvation, timing that aligned to pulse-chase experiments, adult reporter worms were collected and frozen. These worm samples were homogenized, crosslinked, sonicated to shear DNA, and reporter histone protein immunoprecipitated (see Experimental procedures, Fig. S6*A*). As a negative control, the protocol was also performed on N2 wild type worms. Immunoprecipitated DNA was detected in all V5 test ChIP samples but not in the N2 control (Table S1*A*). Input and immunoprecipitated DNA were sequenced to identify genomic regions bound by the histone reporters (see Experimental procedures). Histone reporter peaks were identified in test samples *versus* input and N2 control background (Fig. 3*B*) and were consistent with characteristics typically observed in histone ChIP-seq (38, 39). In addition, multidimensional scaling (MDS) analysis of the identified peaks revealed unique chromatin binding profiles for each histone reporter (Fig. 3*C*). Thus, these

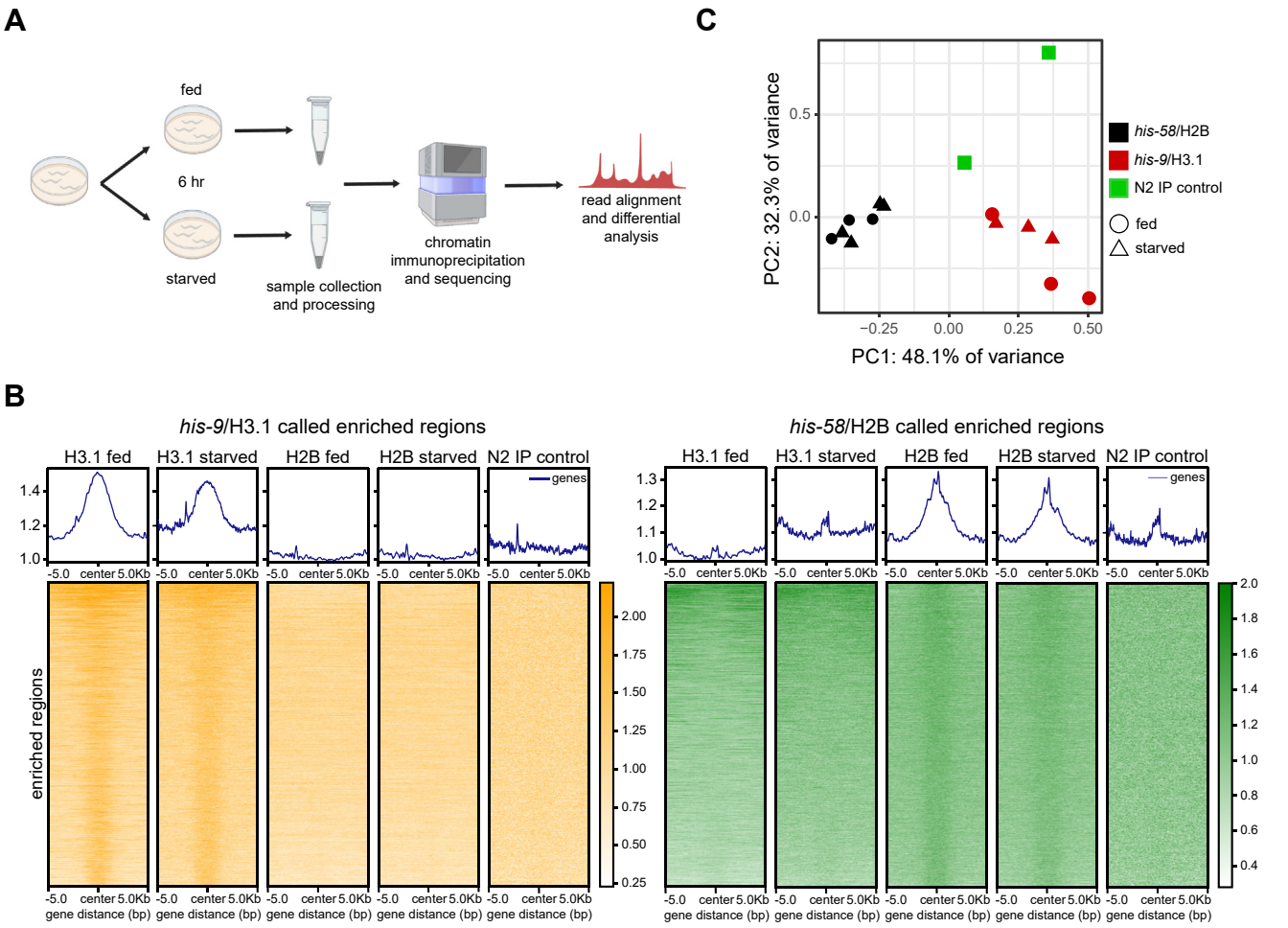

Figure 3. Intestinal histone reporters incorporate into chromatin. *A*, ChIP-seq experimental workflow. Synchronized young adult worms were fed or starved for 6 h prior to sample processing and sequencing. *B*, heatmap of identified *his-9*/H3.1 (*left*) and his-58/H2B (*right*) enriched regions identified by epic2. Enriched regions for his-9/H3.1 are absent in *his-58*/H2B and N2 control. Similarly, enriched regions in *his-58*/H2B were absent in *his-9*/H3.1 and N2 control. *C*, multidimensional scaling (MDS) plot comparing identified enriched regions in *his-9*/H3.1, *his-58*/H2B, and N2 control samples. Samples cluster into respective strain groups. MDS analysis performed using edgeR program. ChIP-seq, chromatin immunoprecipitation and sequencing.

analyses were consistent with functional histone reporter proteins forming specific chromatin interactions in the intestine.

The broad nature of the identified histone peaks made specific gene target identification challenging. Instead, gene targets of the histone reporters were identified by a window-based strategy of signal enrichment within protein coding gene regions previously described for ChIP-seq analysis in other studies (40, 41). Using this strategy, analysis of *his-58*/H2B samples compared to negative controls revealed no significant gene targets, indicating evenly distributed peaks across the genome without specific regional enrichment. When *his-9*/H3.1 samples were compared to negative controls, the analysis identified 187 and 25 genes with significant histone reporter binding in fed and starved samples, respectively (Fig. 4, *A* and *B*; Table S2). All 25 starved targets were present in fed samples (Fig. 4*A*; Table S2). When *his-9*/H3.1 fed and starved samples were compared, no genes with significant changes were identified. Thus, the *his-9*/H3.1 gene targets identified were only specific when compared to the controls, implying no major chromatin changes between animal nutritional states. Tissue enrichment analysis identified that these *his-9*/H3.1 targets enriched for the intestine and other alimentary system related tissues (See Experimental procedures, Fig. 4*C*), while Gene Ontology (GO) enriched for immune and metabolic pathways (See Experimental procedures, Fig. 4*D*), associated functions of the *C. elegans* intestine (42). In sum, ChIP-seq revealed chromatin incorporation of histone reporters. The similarity of *his-9*/H3.1 gene targets between fed and starved animals suggested minimal chromatin changes at this time point of animal starvation.

Discussion

Monitoring the stability and localization of proteins in animals necessitates the ability to label and track a specific protein population across space and time. This work used the HaloTag modified enzyme to establish an *in vivo* protein pulse-chase method in *C. elegans*. HaloTag reporter proteins in the intestine were efficiently labeled by exposing worms to

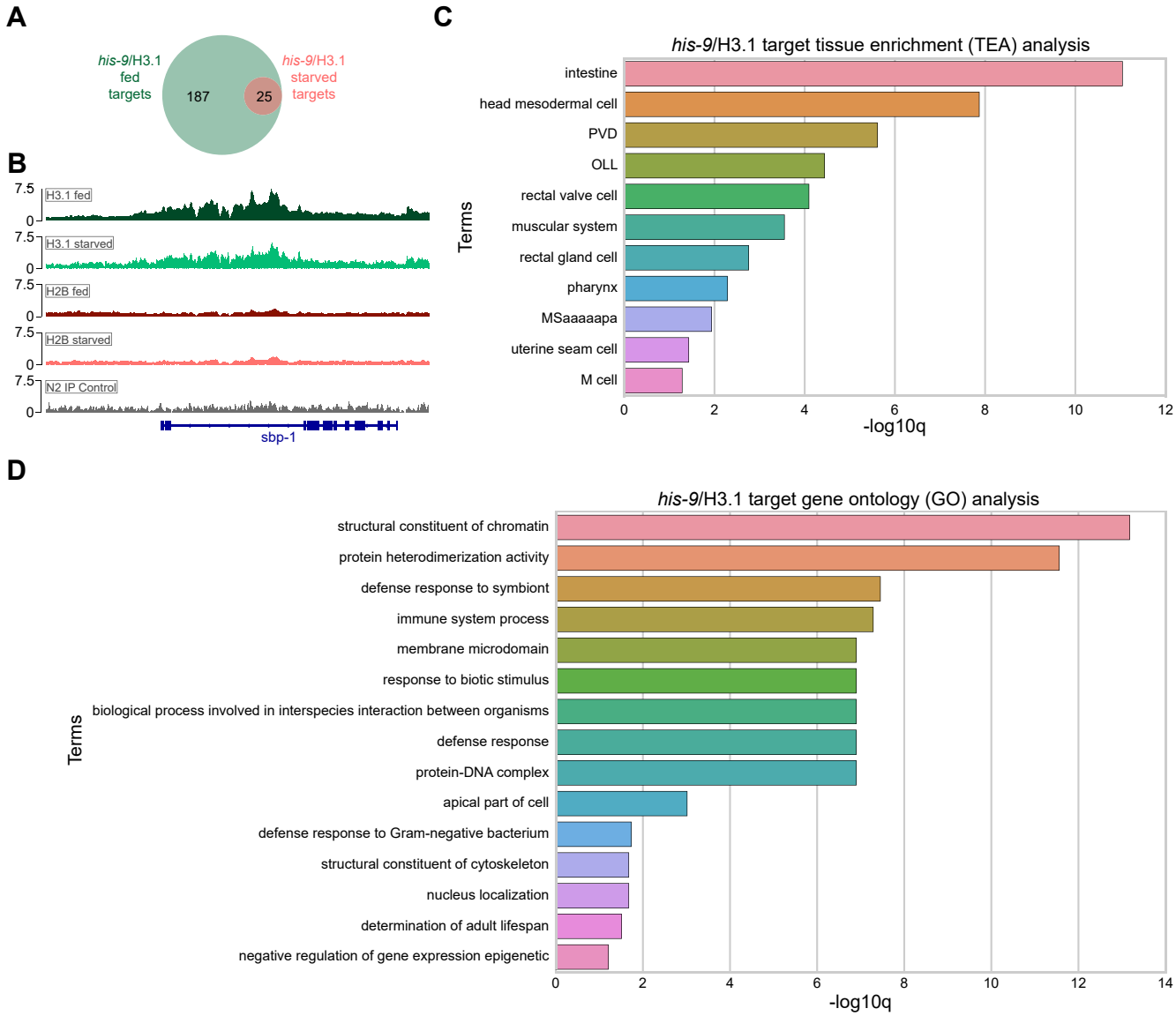

Figure 4. *his-9*/H3.1 identified targets enrich for intestine and intestine-related processes. *A*, 187 genes were identified as *his-9*/H3.1 targets in fed animals and 25 genes were identified as *his-9*/H3.1 targets in starved animals. All 25 starved targets were present in fed samples. *B*, Integrative Genomics Viewer (IGV) (87) browser view of *his-9*/H3.1 identified target, *sbp-1*. Samples were normalized to themselves using the reads per genomic content (RPGC) normalization method. Representative *his-9*/H3.1 fed and starved (*green*), *his-58*/H2B fed and starved (*red*), and N2 control (*gray*) sample shown. *C*, tissue enrichment analysis (TEA) of *his-9*/H3.1 identified targets. Alimentary system tissues enriched in both fed and starved animals. *D*, Gene Ontology analysis (GO) of *his-9*/H3.1 identified targets. Terms in both fed and starved samples reflect alimentary system-related processes.

a fluorescent HaloTag ligand. The stability of these pulse-labeled proteins could be tracked over time in animals, and protein stability was dependent on the animals' nutritional state. Given that the reporter levels were similar in both fed and starved animal conditions, the increase in protein stability also implied a decrease in new protein synthesis. These histone reporter proteins were functional in that they incorporated into chromatin and bound broadly across genes, as expected of histone proteins. Although no targets were able to be identified for histone *his-58*/H2B, histone his-9/H3.1 enriched for genes associated with intestine-associated processes. Thus, this *C. elegans in vivo* pulse-chase method enabled tracking of biologically relevant proteins in specific animal tissue.

HaloTag-based, *in vivo* protein pulse-chase methods have been previously used in cell culture (6, 7, 12, 13) and in mice (8, 14). Although informative, cell culture studies lack the context of authentic tissue, and working in mice elicits both economic and technical challenges. Ensuring reproducible ligand delivery can be difficult and may confound experimental results. This work demonstrated that HaloTag *in vivo* pulse-chase experiments were both straightforward and cost-effective in *C. elegans*. Delivery of the ligand was achieved by soaking the worms in membrane-permeable ligand. The transparent worm also made detection by imaging easy. Limitations also exist. In *C. elegans*, and multicellular animals generally, the current method can only measure protein dynamics on a timescale of hours to days. Studying the stability

and localization of highly dynamic proteins remains a challenge *in vivo*. Efforts to mitigate this limitation include the development of nonfluorescent HaloTag ligands, which can be used in a dual "pulse" strategy to improve labeling time points (12, 43). Challenges of preferential uptake and low membrane permeability for certain tissue (such as the brain) have been reported in mice (8, 44). This work focused on labeling of HaloTag fusion proteins exclusively in the intestine of adult animals. Successful delivery and uptake of ligands by other tissues and during other developmental stages of the worm may be a limitation, which could directly affect labeling efficiency and utility of the method. HaloTag is also a relatively large tag (~33 kDa) and thus requires functional characterization to ensure that the tag does not interfere with protein function. Regardless, the method holds promise to investigate longer lived proteins (45–50) and those that traffic across cells and tissue in animal development (51–53).

Histone H3.1 is well characterized and reported to be deposited into chromatin in a replication-dependent manner (24, 54). The adult *C. elegans* intestine is a nondividing tissue. The organ is fully formed by later developmental stages and serves the animal throughout life (16, 21). Only moderate H3.1 chromatin remodeling may occur during adulthood, which could partially explain the absence of dramatic H3.1 chromatin changes in starved adult animals. The maintenance of specific histones and their associated posttranslational modifications incorporated within the genome is referred to as histone retention. The enriched *his-9*/H3.1 chromatin target GO terms included those involved in chromatin regulation, such as "structural constituent of chromatin," "protein-DNA complex," and "negative regulation of gene expression epigenetic" (Fig. 4*D*). The histone H3.1 targets combined with observations of starvation-induced H3.1 retention potentially suggest epigenetic regulation for metabolic adaptation under nutritional stress. Rather than inducing large-scale chromatin remodeling changes (reviewed in (55)), epigenetic modification of histones themselves may serve as a more rapid response to acute starvation. Indeed, systemic epigenetic histone modification responses to starvation have been reported in *C. elegans* (56, 57) and other organisms (reviewed in (58)) and are important for metabolic adaptation. Metabolism attenuation during starvation relies on the adenosine monophosphate-activated protein kinase (AMPK) as a sensor for nutrient levels (59). Adenosine monophosphate-activated protein kinase is required for *C. elegans* to survive starvation and triggers histone modification to modulate gene expression (57, 60). Investigating essential factors related to nutrient sensing and chromatin regulation may uncover mechanisms related to stabilizing chromatin during periods of nutritional stress.

Alternatively, chromatin remodeling may robustly occur; however, longer starvation periods may be necessary to detect changes in *his-9*/H3.1 chromatin targets. Changes to chromatin architecture in response to starvation are reported in *C. elegans* (35, 61) and other organisms (62). Transcriptomic analyses of *C. elegans* starved for durations similar to this study showed only modest changes compared to those starved for significantly longer periods (42). Furthermore, worms starved for longer periods had chromatin architecture changes in other cell types (35). Future work will investigate the sites of histone chromatin assembly across different types and durations of animal stress states.

Developing methods to study protein dynamics *in vivo* is critical to understanding biological processes *in situ* or their authentic context. This work serves as entrée to illustrate the potential of *in vivo* pulse-chase methodologies in *C. elegans.* From pulse-labeling to detection, the method is highly adaptable to cater investigation into a wide variety of biological processes *in vivo*. For example, proteome dysfunction and aggregation are hallmarks of aging and neurological disorders (63–67). HaloTag pulse-chase could be used to directly observe and measure protein stability and aggregation in the worm. The method could also be applied toward understanding how RNA-protein inheritance dictates transgenerational epigenetic inheritance (reviewed in (68)). Addition of other modified enzyme tags, like SNAP (69), will make it possible to label and track two different proteins of interest simultaneously, further expanding the experimental application. Technical advancements made in *C. elegans* will serve as a stepping-stone to address a variety of questions in metazoan biology.

Experimental procedures

Worm maintenance

C. elegans were grown and maintained on nematode growth medium (NGM; 25 mM KPO4 pH 6.0, 5 mM NaCl, 1 mM $CaCl_2$, 1 mM $MgSO_4$, 2.5 mg/ml tryptone, 5 μg/ml cholesterol, and 1.7% agar) seeded with *Escherichia coli* HB101 as previously reported for standard nematode growth conditions (70). To isolate genomic DNA for genotyping, worms were picked into worm lysis buffer (10 mM Tris–HCl pH 8.3, 50 mM KCl, 2.5 mM $MgCl_2$, 0.45% Triton X-100, 0.45% Tween-20, and 0.01% Gelatin) containing Proteinase K (200 ug/ml) and lysed at 60 °C for 1 h.

Reporter generation

The *elt-2* promoter and genes of interest (*his-9*, *his-58*, and *his-72*, *lmn-1*) were Q5 (NEB, #M0491S) PCR amplified from worm lysate. A *C. elegans* optimized HaloTag (9) was generated by commercial gene fragment synthesis (Twist Biosciences), and the V5 tag (31) was included in PCR primers. Q5 PCR amplified fragments were ligated into pCFJ151 (29) MosSCI vector using Gibson cloning (71). Injections were performed using an Eclipse Ts2 microscope (Nikon), IM-300 Microinjector (Narishige), and Microscope Mechanical Micromanipulator (Leica). EG6699 (*ttTi5605* II) (72) uncs were injected with pDDC14, pDDC15, pDDC16, or pDDC171, somatic red fluorescent protein markers (pGH8, pCFJ90, pCFJ104 (29)), and the germline transposase, pCFJ601 (72) following MosSCI direct insertion protocol (29). The transgenic animals with Mos site insertions rescued the *unc* phenotype (*unc-119*) and lost the somatic red fluorescent protein reporters. Transgene insertion was validated by PCR and proper repair determined by DNA sequencing. All

generated strains were outcrossed twice with N2 worms. See Table S3 for plasmids and strains used in this study.

Pulse labeling

Synchronized reporter worms were washed in PBS + 0.01% Tween-20 (PBS-T) to remove excess bacteria and soaked for 20 min in the presence of 300 nM Halo-TMR (G8251, Promega), Halo-R110Direct (G3221, Promega, G3221), or Halo-Oregon Green (G2801 Promega). Worms incubated without HaloTag ligand served as a negative control. Worms were washed with PBS-T to remove excess ligand. The worms were then further propagated on NGM plates without or with HB101 bacteria, or immediately fixed in 3% paraformaldehyde (50-980-487, Thermo Fisher Scientific) and 100% ice cold methanol (−20 °C). Propagated worms were later collected at specific time points, washed with PBS-T, and fixed as described above. All worms were stained with 1:2000 4′,6-diamidino-2-phenylindole to visualize nuclei and counterstained with a different HaloTag ligand to visualize total reporter protein. Worms pulse-labeled with Halo-TMR were counterstained with Halo-Oregon Green and worms pulse-labeled with either Halo-R110Direct or Halo-Oregon Green were counterstained with Halo-TMR. Samples were pipetted onto slides in Vectashield (H-1900-10, Vector Laboratories Inc), covered with a glass coverslip, and sealed with nail polish. Slides were stored at 4 °C until imaging. Worms were imaged by spinning disk confocal microscopy on a Zeiss Axio Observer Z1 modified by 3i (www.intelligent-imaging.com).

Image processing/quantification

Raw image files were loaded into ImageJ FIJI (73) and fluorescence levels normalized between different ligand groups by setting the fluorescent levels to the same high and low values between all quantified images. To quantify fluorescence, a mask was generated from the Halo counterstain channel image to exclusively mark the intestinal nuclei. The fluorescent threshold levels used for mask generation was maintained between sample groups. The mask was used to quantify the mean fluorescence value of the pulse-labeled Halo ligand channel for the first six nuclei of the intestine. Oversaturated images or poorly outlined nuclei were not used in fluorescence quantitation. Fluorescence quantitation for *lmn-1* reporter animals (*ddcSi43 [elt-2 promoter::lmn-1::histone linker::1xV5::Halo opt with introns::unc-54 3′UTR and intergenic region] II*) followed the same protocol as histone reporters. A mask was generated from the Halo counterstain channel image to mark *lmn-1* puncta in the intestinal nuclei. The mask was used to quantify the mean fluorescence of the pulse-labeled *lmn-1* Halo ligand channel in the first six nuclei of the intestine. Mean fluorescence of *lmn-1* was then compared to the mean fluorescence of CDE6 (*ddcSi2 [elt-2 promoter::his-58::histone linker::1xV5::H. opt with introns::unc-54 3′UTR and intergenic region] II*). Comparison of the fluorescence levels of the different ligands was performed in GraphPad Prism 10.4.1 (GraphPad Software, Inc).

Immunoblots

Histone reporter strains were grown on NGM plates seeded with HB101 bacteria. Plates from each strain were bleached to synchronize strains at the L1 larval stage (74). L1 larvae were plated onto NGM plates with HB101 and grown for 72 h (24 h post L4 stage). Worms were washed from the plate with PBS-T, pipetted into conical tubes, and washed with PBS-T to remove remaining bacteria. After the final wash, the samples were pipetted onto NGM plates without or with HB101. These samples were incubated for 6 h at 20 °C and again washed with PBS-T to remove bacteria. Samples were transferred to tubes with 5x SDS-PAGE sample buffer (250 mM Tris pH 6.8, 25 mM EDTA pH 8.0, 25% glycerol, and 5% SDS), frozen at −80 °C, and stored at −20 °C until use. Samples were run on SDS-PAGE gel and transferred to polyvinylidene fluoride (Bio-Rad, #1620264) using the Bio-Rad TransBlot Turbo System (Bio-Rad, #1704150). Blots were probed with a primary anti-V5 monoclonal antibody (R&D Systems Bio-techne-NBP1-80562) and secondary goat-anti-mouse horseradish peroxidase antibody (VWR, #95058-740) prior to incubation in SuperSignal Plus West Femto (Thermo Fisher Scientific, #34094) and SuperSignal Plus West Pico (Thermo Fisher Scientific, #34580). Blots were imaged on a Bio-Rad ChemiDoc MP system (Bio-Rad, #12003154). Blots were stripped and reprobed with a primary anti-GAPDH antibody (60004-1-Ig) and secondary goat-anti-mouse horseradish peroxidase antibody (VWR, #95058-740). Chemiluminescence exposure settings were kept identical between replicate blots to maintain reproducibility. V5 and GAPDH antibodies commercially available and validated by Novus Biologicals and Proteintech, respectively.

Quantification of protein bands was performed using Image Lab (Bio-Rad) and ImageJ FIJI (73). In Image Lab, chemiluminescent image contrast was adjusted to optimal, identical levels. ImageJ FIJI was used to determine band density. Relative protein expression of the histone reporters was determined by a quotient of histone reporter over GAPDH loading control band density. Statistical significance was determined using a two-way analysis of variance (ANOVA) and Tukey's multiple comparisons test in GraphPad Prism 10.4.1 (GraphPad Software, Inc).

Chromatin immunoprecipitation and sequencing

Sample collection

CDE5, CDE6, and N2 worms were bleached for a synchronous population of L1 larvae (74). L1s were pipetted onto NGM plates with concentrated HB101 and propagated for 72 h. Worms were collected and washed with PBS-T to remove bacteria then added to concentrated HB101 or empty plates. These worms were fed or starved for 6 h, collected, washed with PBS-T, and samples frozen in liquid nitrogen. Frozen samples were stored at −80 °C until processing.

ChIP protocol

ChIP-seq sample preparation protocol was modeled from Sen *et al.* with modifications (75). Frozen worms were lysed

ASBMB

by a prechilled BioPulverizer (Biospec, #59013N). Pulverized samples were moved to a prechilled mortar and grinded vigorously with mortar and pestle (Thermo Fisher Scientific, #FB961B; #FB961L). Sample powder was moved to tubes and reconstituted in Nuclei Preparation Buffer (10 mM Hepes pH 7.5, 10 mM KCl, 1.5 mM $MgCl_2$, and 0.1% Triton X-100) containing protease inhibitors (Promega, #G6521). Samples were cross-linked in 1.1% paraformaldehyde (Thermo Fisher Scientific, #50-980-487) for 4 min and quenched for 10 min with 125 mM (final concentration) Glycine (VWR, #97061-128). Samples were washed in Nuclei Preparation Buffer + protease inhibitors and resuspended in lysis buffer (50 mM Tris pH 8.1, 10 mM EDTA, and 0.25% SDS) plus protease inhibitors. A Diagenode Bioruptor Plus sonicator (#B01020001) and TPX tubes (Diagenode, #NC0065146) were used to sonicate samples to generate 400 to 500 bp DNA fragments. Sonicated samples were centrifuged, supernatant removed, and its protein concentration determined by Bradford analysis (Bio-Rad, #5000006). Samples were taken as a protein and DNA input control. The immunoprecipitation (IP) was performed by calculating the volume of sample needed for 1 mg of total input protein. This volume was diluted by half using broad nuclei lysis buffer (10 mM Tris–HCl pH 7.5, 1% Triton X-100, 0.5% Na deoxycholate, 0.1% SDS). ChIP dilution buffer (16.7 mM Tris–HCl pH 8.1, 1.1% Triton X-100, and 167 mM NaCl, 1.2 mM EDTA, and 0.01% SDS) was added to obtain a final IP volume of 2 mls. Subsequently, 2 μg of anti-V5 mouse monoclonal antibody (R&D Systems Bio-Techne-NBP1-80562) was added and incubated overnight at 4 °C with rotation. The next morning, Protein G dynabeads (Invitrogen, #10-003-D) were washed with blocking buffer (1x PBS+0.5% Tween, 0.5% bovine serum albumin plus protease inhibitor) and added to IP samples and incubated for 1 h at 4 °C with rotation. IP samples were washed with radioimmunoprecipitation assay low (20 mM Tris–HCl pH 8.1, 140 mM NaCl, 1 mM EDTA, 0.1% SDS, 1% Triton x-100, and 0.1% DOC), radioimmunoprecipitation assay high (20 mM Tris–HCl pH 8.1, 500 mM NaCl, 1 mM EDTA, 0.1% SDS, 1% Triton x-100, 0.1% DOC), LiCl (10 mM Tris–HCl pH 8.1, 250 mM LiCl, 1 mM EDTA 0.5%, Triton X-100, 0.5% DOC), and Tris-EDTA buffer (10 mM Tris–HCl pH 8.0, 1 mM EDTA). Samples were placed into elution buffer (10 mM Tris–HCl pH 8.0, 300 mM NaCl, 5 mM EDTA, 0.1% SDS, and 5 mM DTT) containing 5 mg/ml Proteinase K (NEB, #P8107S) and 62.5 μg/ml RNAse A (Sigma-Aldrich, #R6513-50MG), and cross-links were reversed overnight by incubation at 37 °C. DNA was purified using AMPure XP beads (Beckman Coulter, #A63880) protocol, and concentration was determined by Qubit analysis (Thermo Fisher Scientific, #Q33238). Input and IP sequencing libraries were generated using the NEBNext Ultra II DNA Library Prep Kit for Illumina (NEB, #E7645S) with barcodes unique to each of the samples (NEB, #E7335S; #E7500S). Samples were pooled and sequenced using the NextSeq 2000 (200 cycles, 400M total reads) at the Indiana University Center for Medical Genomics Core Facility. All ChIP-seq experiments were repeated at least three times.

Sequencing analyses

Fastq raw sequencing files were assessed for quality and filtered to remove adaptors by fastp (76). Filtered reads were aligned to the *C. elegans* genome using Bowtie 2 (77) with WBcel235 (*ce11*) as the reference genome. Read alignments were further processed using SAMtools (78) to remove duplicate and mitochondrial reads and BEDTools (79) to remove any "blacklisted" alignments found in the *C. elegans* genome (UCSC). Samples with low read counts were excluded from downstream analysis: IP samples with read count of less than 15 million and input samples with read count less than nine million. deepTools (80) was used to generate bigwig files for visualization of enriched regions on genome browsers (Fig. 4*B*). To visualize chromatin incorporation, enriched regions were identified using epic2, a program efficient at identifying diffuse ChIP-seq domains (81). Background enriched regions were identified in N2 controls and filtered from histone samples using BEDTools (79). All filtered enriched regions from histone samples were used to generate heatmaps to visualize the genome-wide enrichment profile of specific histone variants using Deeptools (Fig. 3B) (80). MDS analysis was performed in edgeR. Enriched regions called by epic2 in all samples (*his-58*, *his-9*, and N2 IP control) were combined into a union set using BEDTools and reads in all enriched regions counted by featureCounts (82). Count files were then used in edgeR to generate MDS plot (Fig. 3*C*). Genomic targets of histone variants in fed and starved samples were identified by performing edgeR differential analysis comparing reads from histone reporter samples to inputs and N2 IgG controls (83), applying a cutoff of a $\log_2$ fold change ($\log_2$FC) greater than one and false discovery rate of less than or equal to 0.05. Read counts at each protein coding gene locus were determined using featureCounts with the protein coding gene coordinates as the input (84, 85). Tissue enrichmentand GO analyses was performed using the WormBase Bioinformatics tool (Fig. 4, *C* and *D*) (86). For differential analysis between fed and starved histone reporters, the genomic coordinates of all *C. elegans* protein coding genes was used as an identifier (84, 85). The number of reads on all protein coding genes in each sample was determined using featureCounts (82). Reads between fed and starved samples were compared using edgeR (83), applying a cutoff of a $\log_2$ fold change ($\log_2$FC) greater than one and a false discovery rate of less than or equal to 0.05 to identify gene targets with significant enrichment changes. Raw sequencing reads and processed data for genome browser visualization are available at the Gene Expression Omnibus website, www.ncbi.nlm.nih.gov/geo, under accession ID GSE289739.

Data availability

All worm strains are available through the *Caenorhabditis* Genetics Center (CGC) or by request. Raw image and

immunoblot files are also available by request. All raw ChIP-seq sequencing data are available through the Gene Expression omnibus (GEO; Entry ID: GSE289739).

Supporting information—This article contains supporting information.

Acknowledgments—The authors thank D. Rusch of the Center for Genomics and Bioinformatics (Indiana University Bloomington) for help with ChIP-seq analyses and members of the Aoki and Roh laboratories for helpful discussion. The Center for Medical Genomics at the Indiana University School of Medicine assisted in DNA sequencing and is partially supported by the Indiana University Grand Challenges Precision Health Initiative (PHI).

Author contributions—C. B., K. O., H. C. R., and S. T. A. writing–review and editing; C. B., K. O., and S. T. A. investigation; C. B., K. O., and S. T. A. resources; C. B., K. O., and S. T. A. writing–original draft; C. B., H. C. R., and S. T. A. validation; C. B., H. C. R., and S. T. A. data curation; C. B., H. C. R., and S. T. A. formal analysis; C. B. and H. C. R. software; C. B. and S. T. A. visualization; H. C. R. and S. T. A. supervision; H. C. R. and S. T. A. methodology; S. T. A. investigation; S. T. A. project administration; S. T. A. funding acquisition; S. T. A. conceptualization.

Funding and additional information—H. R. is supported by the National Institute of Diabetes and Digestive and Kidney Diseases (R01DK129289) and American Diabetes Association Junior Faculty Award (7-21-JDF-056). S. T. A. and this work was funded by the Indiana University School of Medicine Precision Health Initiative, Showalter Trust, and the National Institute of General Medical Sciences (R35GM142691). The content is solely the responsibility of the authors and does not necessarily represent the official views of the National Institutes of Health.

Conflict of interest—The authors declare that they have no conflicts of interest with the contents of this article.

Abbreviations—The abbreviations used are: ChIP-seq, Chromatin immunoprecipitation and sequencing; GO, Gene Ontology; IP, Immunoprecipitation; MDS, Multidimensional scaling; NGM, Nematode growth medium; PBS-T, PBS + 0.01% Tween-20.

References

1. Backwell, L., and Marsh, J. A. (2022) Diverse molecular mechanisms underlying pathogenic protein mutations: beyond the loss-of-function paradigm. *Annu. Rev. Genomics Hum. Genet.* **23**, 475–498
2. Enticknap, J. B. (1958) Absorption of radioactive bacteria labelled With35s methionine from the appendix of the rabbit. *Q. J. Exp. Physiol. Cogn. Med. Sci.* **43**, 169–173
3. Tarver, H., and Reinhardt, W. O. (1947) Methionine labeled with radioactive sulfur as an indicator of protein formation in the hepatectomized dog. *J. Biol. Chem.* **167**, 395–400
4. Tarver, H., and Schmidt, C. L. A. (1942) Radioactive sulfur studies. *J. Biol. Chem.* **146**, 69–84
5. Schoenheimer, R., Rittenberg, D., Foster, G. L., Keston, A. S., and Ratner, S. (1938) The application of the nitrogen isotope N15 for the study of protein metabolism. *Science* **88**, 599–600
6. Jansen, L. E., Black, B. E., Foltz, D. R., and Cleveland, D. W. (2007) Propagation of centromeric chromatin requires exit from mitosis. *J. Cell Biol.* **176**, 795–805
7. Foltz, D. R., Jansen, L. E., Bailey, A. O., Yates, J. R., 3rd, Bassett, E. A., Wood, S., *et al.* (2009) Centromere-specific assembly of CENP-a nucleosomes is mediated by HJURP. *Cell* **137**, 472–484
8. Bojkowska, K., Santoni de Sio, F., Barde, I., Offner, S., Verp, S., Heinis, C., *et al.* (2011) Measuring in vivo protein half-life. *Chem. Biol.* **18**, 805–815
9. Los, G. V., Encell, L. P., McDougall, M. G., Hartzell, D. D., Karassina, N., Zimprich, C., *et al.* (2008) HaloTag: a novel protein labeling technology for cell imaging and protein analysis. *ACS Chem. Biol.* **3**, 373–382
10. Erdmann, R. S., Baguley, S. W., Richens, J. H., Wissner, R. F., Xi, Z., Allgeyer, E. S., *et al.* (2019) Labeling strategies matter for super-resolution microscopy: a comparison between HaloTags and SNAP-tags. *Cell Chem. Biol.* **26**, 584–592.e6
11. Hoelzel, C. A., and Zhang, X. (2020) Visualizing and manipulating biological processes by using HaloTag and SNAP-tag technologies. *Chembiochem* **21**, 1935–1946
12. Merrill, R. A., Song, J., Kephart, R. A., Klomp, A. J., Noack, C. E., and Strack, S. (2019) A robust and economical pulse-chase protocol to measure the turnover of HaloTag fusion proteins. *J. Biol. Chem.* **294**, 16164–16171
13. Fritzsche, S., and Springer, S. (2014) Pulse-chase analysis for studying protein synthesis and maturation. *Curr. Protoc. Protein Sci.* **78**, 30.3.1–30.3.23
14. Bulovaite, E., Qiu, Z., Kratschke, M., Zgraj, A., Fricker, D. G., Tuck, E. J., *et al.* (2022) A brain atlas of synapse protein lifetime across the mouse lifespan. *Neuron* **110**, 4057–4073.e8
15. Meneely, P. M., Dahlberg, C. L., and Rose, J. K. (2019) Working with worms: Caenorhabditis elegans as a model organism. *Curr. Protoc. Essent. Lab. Tech.* **19**, 1–35
16. Dimov, I., and Maduro, M. F. (2019) The C. elegans intestine: organogenesis, digestion, and physiology. *Cell Tissue Res.* **377**, 383–396
17. Peres, T. V., Arantes, L. P., Miah, M. R., Bornhorst, J., Schwerdtle, T., Bowman, A. B., *et al.* (2018) Role of Caenorhabditis elegans AKT-1/2 and SGK-1 in manganese toxicity. *Neurotox. Res.* **34**, 584–596
18. Tan, M.-W., Block, D. H. S., Twumasi-Boateng, K., Kang, H. S., Carlisle, J. A., Hanganu, A., *et al.* (2015) The developmental intestinal regulator ELT-2 controls p38-dependent immune responses in adult C. elegans. *PLoS Genet.* **11**, e1005265.
19. Pukkila-Worley, R., and Ausubel, F. M. (2012) Immune defense mechanisms in the Caenorhabditis elegans intestinal epithelium. *Curr. Opin. Immunol.* **24**, 3–9
20. Kimble, J., and Sharrock, W. J. (1983) Tissue-specific synthesis of yolk proteins in Caenorhabditis elegans. *Dev. Biol.* **96**, 189–196
21. Sulston, J. E., and Horvitz, H. R. (1977) Post-embryonic cell lineages of the nematode, Caenorhabditis elegans. *Dev. Biol.* **56**, 110–156
22. Hedgecock, E. M., and White, J. G. (1985) Polyploid tissues in the nematode Caenorhabditis elegans. *Dev. Biol.* **107**, 128–133
23. Son, M., Kawasaki, I., Oh, B.-K., and Shim, Y.-H. (2016) LIN-23, an E3 ubiquitin ligase component, is required for the repression of CDC-25.2 activity during intestinal development in Caenorhabditis elegans. *Mol. Cells* **39**, 834–840
24. Henikoff, S., and Smith, M. M. (2015) Histone variants and epigenetics. *Cold Spring Harb Perspect. Biol.* **7**, a019364
25. Luger, K., Mäder, A. W., Richmond, R. K., Sargent, D. F., and Richmond, T. J. (1997) Crystal structure of the nucleosome core particle at 2.8 Å resolution. *Nature* **389**, 251–260
26. Cui, M., and Han, M. (2007) Roles of chromatin factors in C. elegans development. *WormBook* **3**, 1–16
27. Morrison, A. J. (2020) Chromatin-remodeling links metabolic signaling to gene expression. *Mol. Metab.* **38**, 100973
28. Horowitz, B. B., Nanda, S., and Walhout, A. J. M. (2023) A transcriptional cofactor regulatory network for the C. elegans intestine. *G3 (Bethesda)* **13**, jkad096
29. Frøkjær-Jensen, C., Wayne Davis, M., Hopkins, C. E., Newman, B. J., Thummel, J. M., Olesen, S.-P., *et al.* (2008) Single-copy insertion of transgenes in Caenorhabditis elegans. *Nat. Genet.* **40**, 1375–1383

30. Fukushige, T., Hawkins, M. G., and McGhee, J. D. (1998) The GATA-factor elt-2 is essential for formation of the Caenorhabditis elegans intestine. *Dev. Biol.* **198**, 286–302
31. Southern, J. A., Young, D. F., Heaney, F., Baumgartner, W. K., and Randall, R. E. (1991) Identification of an epitope on the P and V proteins of simian virus 5 that distinguishes between two isolates with different biological characteristics. *J. Gen. Virol.* **72**, 1551–1557
32. Buchwalter, A. (2023) Intermediate, but not average: the unusual lives of the nuclear lamin proteins. *Curr. Opin. Cell Biol.* **84**, 102220
33. Hasper, J., Welle, K., Hryhorenko, J., Ghaemmaghami, S., and Buchwalter, A. (2023) Turnover and replication analysis by isotope labeling (TRAIL) reveals the influence of tissue context on protein and organelle lifetimes. *Mol. Syst. Biol.* **19**, e11393
34. Liu, J., Ben-Shahar, T. R., Riemer, D., Treinin, M., Spann, P., Weber, K., *et al.* (2000) Essential roles for Caenorhabditis elegansLamin gene in nuclear organization, cell cycle progression, and spatial organization of nuclear pore complexes. *Mol. Biol. Cell* **11**, 3937–3947
35. Zhu, Z., Li, D., Jia, Z., Zhang, W., Chen, Y., Zhao, R., *et al.* (2023) Global histone H2B degradation regulates insulin/IGF signaling-mediated nutrient stress. *EMBO J.* **42**, e113328
36. Kim, U., and Lee, D.-S. (2023) Epigenetic regulations in mammalian cells: roles and profiling techniques. *Mol. Cells* **46**, 86–98
37. Kimura, H. (2013) Histone modifications for human epigenome analysis. *J. Hum. Genet.* **58**, 439–445
38. Chen, Y., Bravo, J. I., Son, J. M., Lee, C., and Benayoun, B. A. (2020) Remodeling of the H3 nucleosomal landscape during mouse aging. *Transl Med. Aging* **4**, 22–31
39. Palma, F. R., Coelho, D. R., Pulakanti, K., Sakiyama, M. J., Huang, Y., Ogata, F. T., *et al.* (2024) Histone H3.1 is a chromatin-embedded redox sensor triggered by tumor cells developing adaptive phenotypic plasticity and multidrug resistance. *Cell Rep.* **43**, 113897
40. Lun, A. T., and Smyth, G. K. (2014) De novo detection of differentially bound regions for ChIP-seq data using peaks and windows: controlling error rates correctly. *Nucleic Acids Res.* **42**, e95
41. Eder, T., and Grebien, F. (2022) Comprehensive assessment of differential ChIP-seq tools guides optimal algorithm selection. *Genome Biol.* **23**, 119
42. Harvald, E. B., Sprenger, R. R., Dall, K. B., Ejsing, C. S., Nielsen, R., Mandrup, S., *et al.* (2017) Multi-omics analyses of starvation responses reveal a central role for lipoprotein metabolism in acute starvation survival in C. elegans. *Cell Syst.* **5**, 38–52.e34
43. Cohen, L. D., Boulos, A., and Ziv, N. E. (2020) A non-fluorescent HaloTag blocker for improved measurement and visualization of protein synthesis in living cells. *F1000Res* **9**, 1–20
44. Tseng, J.-C. (2013) In Vivo fluorescent labeling of tumor cells with the HaloTag technology. *Curr. Chem. Genomics* **6**, 48–54
45. Savas, J. N., Toyama, B. H., Xu, T., Yates, J. R., and Hetzer, M. W. (2012) Extremely long-lived nuclear pore proteins in the rat brain. *Science* **335**, 942
46. Toyama, B. H., Savas, J. N., Park, S. K., Harris, M. S., Ingolia, N. T., Yates, J. R., *et al.* (2013) Identification of long-lived proteins reveals exceptional stability of essential cellular structures. *Cell* **154**, 971–982
47. Fornasiero, E. F., Mandad, S., Wildhagen, H., Alevra, M., Rammner, B., Keihani, S., *et al.* (2018) Precisely measured protein lifetimes in the mouse brain reveal differences across tissues and subcellular fractions. *Nat. Commun.* **9**, 4230
48. Krishna, S., Arrojo e Drigo, R., Capitanio, J. S., Ramachandra, R., Ellisman, M., and Hetzer, M. W. (2021) Identification of long-lived proteins in the mitochondria reveals increased stability of the electron transport chain. *Dev. Cell* **56**, 2952–2965.e9
49. Heo, S., Diering, G. H., Na, C. H., Nirujogi, R. S., Bachman, J. L., Pandey, A., *et al.* (2018) Identification of long-lived synaptic proteins by proteomic analysis of synaptosome protein turnover. *Proc. Natl. Acad. Sci. U. S. A.* **115**
50. Erinjeri, A. P., and Labbadia, J. (2021) The importance of long-lived proteins: not just nuclear anymore. *Dev. Cell* **56**, 2925–2927
51. Eroglu, M., Zocher, T., McAuley, J., Webster, R., Xiao, M. Z. X., Yu, B., *et al.* (2024) Noncanonical inheritance of phenotypic information by protein amyloids. *Nat. Cell Biol.* **26**, 1712–1724
52. Harvey, Z. H., Chen, Y., and Jarosz, D. F. (2018) Protein-based inheritance: epigenetics beyond the chromosome. *Mol. Cell* **69**, 195–202
53. Kreissl, F. K., Banki, M. A., and Droujinine, I. A. (2022) Molecular methods to study protein trafficking between organs. *Proteomics* **23**, e2100331
54. Sokolova, V., Sarkar, S., and Tan, D. (2023) Histone variants and chromatin structure, update of advances. *Comput. Struct. Biotechnol. J.* **21**, 299–311
55. Zhou, C. Y., Johnson, S. L., Gamarra, N. I., and Narlikar, G. J. (2016) Mechanisms of ATP-dependent chromatin remodeling motors. *Annu. Rev. Biophys.* **45**, 153–181
56. Rechavi, O., Houri-Ze'evi, L., Anava, S., Goh, Wee Siong S., Kerk, Sze Y., Hannon, Gregory J., *et al.* (2014) Starvation-induced transgenerational inheritance of small RNAs in C. elegans. *Cell* **158**, 277–287
57. Sun, B., Sherrin, M., and Roy, R. (2023) Unscheduled epigenetic modifications cause genome instability and sterility through aberrant R-loops following starvation. *Nucleic Acids Res.* **51**, 84–98
58. González-Rodríguez, P., Füllgrabe, J., and Joseph, B. (2023) The hunger strikes back: an epigenetic memory for autophagy. *Cell Death Differ.* **30**, 1404–1415
59. Hardie, D. G., Ross, F. A., and Hawley, S. A. (2012) AMPK: a nutrient and energy sensor that maintains energy homeostasis. *Nat. Rev. Mol. Cell Biol.* **13**, 251–262
60. Demoinet, E., Li, S., and Roy, R. (2017) AMPK blocks starvation-inducible transgenerational defects in Caenorhabditis elegans. *Proc. Natl. Acad. Sci U. S. A.* **114**, E2689–E2698
61. Riedel, C. G., Dowen, R. H., Lourenco, G. F., Kirienko, N. V., Heimbucher, T., West, J. A., *et al.* (2013) DAF-16 employs the chromatin remodeller SWI/SNF to promote stress resistance and longevity. *Nat. Cell Biol.* **15**, 491–501
62. Bieluszewski, T., Prakash, S., Roulé, T., and Wagner, D. (2023) The role and activity of SWI/SNF chromatin remodelers. *Annu. Rev. Plant Biol.* **74**, 139–163
63. Roussos, A., Kitopoulou, K., Borbolis, F., and Palikaras, K. (2023) Caenorhabditis elegans as a model system to study human neurodegenerative disorders. *Biomolecules* **13**, 478
64. Zhang, S., Li, F., Zhou, T., Wang, G., and Li, Z. (2020) Caenorhabditis elegans as a useful model for studying aging mutations. *Front. Endocrinol.* **11**, 554994
65. Nakamura, T., Tu, S., Akhtar, M. W., Sunico, C. R., Okamoto, S.-I., and Lipton, S. A. (2013) Aberrant protein s-nitrosylation in neurodegenerative diseases. *Neuron* **78**, 596–614
66. Lee, E., Park, H., and Kim, S. (2024) Transcellular transmission and molecular heterogeneity of aggregation-prone proteins in neurodegenerative diseases. *Mol. Cells* **47**, 100089
67. Campioni, S., Mannini, B., Zampagni, M., Pensalfini, A., Parrini, C., Evangelisti, E., *et al.* (2010) A causative link between the structure of aberrant protein oligomers and their toxicity. *Nat. Chem. Biol.* **6**, 140–147
68. Sundby, A. E., Molnar, R. I., and Claycomb, J. M. (2021) Connecting the dots: linking *Caenorhabditis elegans* small RNA pathways and germ granules. *Trends Cell Biol.* **31**, 387–401
69. Keppler, A., Gendreizig, S., Gronemeyer, T., Pick, H., Vogel, H., and Johnsson, K. (2002) A general method for the covalent labeling of fusion proteins with small molecules in vivo. *Nat. Biotechnol.* **21**, 86–89
70. Brenner, S. (1974) The Genetics of Caenorhabditis elegans. *Genetics* **77**, 71–94
71. Gibson, D. G., Young, L., Chuang, R.-Y., Venter, J. C., Hutchison, C. A., and Smith, H. O. (2009) Enzymatic assembly of DNA molecules up to several hundred kilobases. *Nat. Methods* **6**, 343–345
72. Frøkjær-Jensen, C., Davis, M. W., Ailion, M., and Jorgensen, E. M. (2012) Improved Mos1-mediated transgenesis in C. elegans. *Nat. Methods* **9**, 117–118

73. Schindelin, J., Arganda-Carreras, I., Frise, E., Kaynig, V., Longair, M., Pietzsch, T., *et al.* (2012) Fiji: an open-source platform for biological-image analysis. *Nat. Methods* **9**, 676–682
74. Stiernagle, T. (2006) Maintenance of C. elegans. *WormBook*. https://doi.org/10.1895/wormbook.1.101.1
75. Sen, I., Kavšek, A., and Riedel, C. G. (2021) Chromatin immunoprecipitation and sequencing (ChIP-seq) optimized for application in Caenorhabditis elegans. *Curr. Protoc.* **1**, e187
76. Chen, S., Zhou, Y., Chen, Y., and Gu, J. (2018) fastp: an ultra-fast all-in-one FASTQ preprocessor. *Bioinformatics* **34**, i884–i890
77. Langmead, B., and Salzberg, S. L. (2012) Fast gapped-read alignment with Bowtie 2. *Nat. Methods* **9**, 357–359
78. Li, H., Handsaker, B., Wysoker, A., Fennell, T., Ruan, J., Homer, N., *et al.* (2009) The sequence alignment/map format and SAMtools. *Bioinformatics* **25**, 2078–2079
79. Quinlan, A. R., and Hall, I. M. (2010) BEDTools: a flexible suite of utilities for comparing genomic features. *Bioinformatics* **26**, 841–842
80. Ramírez, F., Dündar, F., Diehl, S., Grüning, B. A., and Manke, T. (2014) deepTools: a flexible platform for exploring deep-sequencing data. *Nucleic Acids Res.* **42**, W187–W191
81. Stovner, E. B., Sætrom, P., and Hancock, J. (2019) epic2 efficiently finds diffuse domains in ChIP-seq data. *Bioinformatics* **35**, 4392–4393
82. Liao, Y., Smyth, G. K., and Shi, W. (2014) featureCounts: an efficient general purpose program for assigning sequence reads to genomic features. *Bioinformatics* **30**, 923–930
83. Robinson, M. D., McCarthy, D. J., and Smyth, G. K. (2010) edgeR: a Bioconductor package for differential expression analysis of digital gene expression data. *Bioinformatics* **26**, 139–140
84. Martin, F. J., Amode, M. R., Aneja, A., Austine-Orimoloye, O., Azov, A. G., Barnes, I., *et al.* (2023) Ensembl 2023. *Nucleic Acids Res.* **51**, D933–D941
85. Smedley, D., Haider, S., Ballester, B., Holland, R., London, D., Thorisson, G., *et al.* (2009) BioMart – biological queries made easy. *BMC Genomics* **10**, 22
86. Angeles-Albores, D., RY, N. L., Chan, J., and Sternberg, P. W. (2016) Tissue enrichment analysis for C. elegans genomics. *BMC Bioinformatics* **17**, 366
87. Robinson, J. T., Thorvaldsdottir, H., Winckler, W., Guttman, M., Lander, E. S., Getz, G., *et al.* (2011) Integrative genomics viewer. *Nat. Biotechnol.* **29**, 24–26